LANDMINE DETECTION IN HIGH RESOLUTION 3D GPR IMAGES

E.E. Ligthart*, A. G. Yarovoy, F. Roth, L.P. Ligthart FIEEE

Abstract—*This paper describes a novel landmine detection and classification algorithm for high resolution 3D ground penetrating radar (GPR) images. The algorithm was tested on data measured with a video impulse radar (VIR) system developed by the International Research Centre for Telecommunications-transmission and Radar (IRCTR). The algorithm detected all landmines (including the difficult to detect M14 mines) and classified almost all specific landmines features correctly with a reasonably low false alarm rate. The feature on a small height object demonstrates an effective reduction of false alarms.*

Keywords: Ground penetrating radar; Image processing; Object detection; Classification

I. INTRODUCTION

Improving detectability and decreasing the false alarm rate of a GPR sensor for landmine detection is a main objective of numerous researches in the past years. The importance of this paper lies in reducing the false alarm rate and obtaining a better performance than existing methods in landmine detection.

Research on landmine detection starting from a two-dimensional (2D) energy projection of a SAR image volume has been reported in [1]. Object detection and classification of landmines in 2D images [2], using 3D image analysis and object visualization have been performed [3]. However, to our knowledge 3D landmine detection and classification is new in GPR images using their 3D nature.

The goal of this paper is to elucidate the developed algorithm that meets the following demands:

- All recognizable landmines should be detected.
- A low number of false alarms is required.
- Known 2D image processing methods should be extended to 3D. All image dimensions should be used for detection and classification.
- The performance of the algorithm should be validated based on actual GPR measurements.

Section II summarizes the acquisition and preprocessing of the data. Section III presents the detection procedure for 3D GPR images. The classification procedure is addressed in detail in Section IV. The results and a discussion of the performance are given in Section V. Finally; the paper ends with conclusions and some recommendations in Section VI.

II. GENERATION OF 3D GPR IMAGES AND THEIR PROPERTIES

During the measurement campaign [4] the GPR system has been mounted on the relocatable scanner of Delft University. It scans over a dry sandy lane along one axis measuring successive A-scans every 1 cm and adds them to parallel B-scans along the other axis with an interval of 1 cm as well. The used measured area is 170cm by 196cm and 20cm in depth. Two types of landmines are buried: PMN mines (medium metal content, diameter: 11.2cm) and M14 mines (very low metal content, diameter: 5.6cm). In total, 13 wanted targets are buried: 6 PMN mines, 6 M14 mines and one unintentionally man-made object with a strong resemblance to a landmine radar image. Further, some false alarms like stones, bottle and wire are intentionally buried. All other objects are referred to as clutter and are unwanted in the detection and classification process.

The GPR system that was used to acquire the data is the polarimetric Video Impulse Radar (VIR) system [5]. This system is developed by IRCTR and is dedicated to landmine detection in the ground subsurface. The VIR system consists of 2 transmit antennas and 4 receive antennas. For further information about the VIR system allowing mono-/multi-static, co-/cross-polar operational modes one is referred to [5].

The acquired data are preprocessed to remove system instabilities, to reduce clutter and to get a better object position accuracy before the 3D imaging is performed by applying SAR processing techniques [6].

Properties of 3D radar images of wanted targets that discriminate them from clutter are the rotationally symmetric amplitude distribution of wanted target images in horizontal cross sections, the high amplitudes and the appearance in many depth slices (the total measured depth of 20cm is sampled with 0.25cm steps resulting in 80 depth slices).

* International Research Centre for Telecommunications-transmission and Radar (IRCTR), Delft University of Technology, Mekelweg 4, 2628 CD Delft, The Netherlands, email: E.E.Ligthart@its.tudelft.nl

III. Object Detection

Before object detection is applied, the envelope of each A-scan is computed in order to eliminate zero crossings and negative amplitudes.

To detect the wanted targets from the 3D image, an adaptive threshold technique is used to establish different threshold levels for each depth slice of the 3D image. The reason for this is that the amount of clutter is much higher in depth slices around the residuals of the surface reflection than in other depth slices.

For each depth slice the amount of detected objects is computed and plotted versus the accompanying threshold value. The resulting curves are different for each depth slice, but have roughly the same shape (see Fig. 1 for a depth slice with less clutter and a depth slice with much clutter). It turned out that the best performance of the threshold value occurs at around 30% of the maximum in the curve.

The 3D binary result after applying the adaptive threshold procedure is shown in Fig. 2. Not only the wanted targets are detected, but also surface clutter and other unwanted objects. Therefore classification is needed to eliminate the clutter and to obtain a low amount of false alarms.

IV. Object Classification

Before classification, size-based clutter removal has been applied. For classification of the objects, features are extracted with selective properties in favor of the wanted targets.

A. Size-based clutter removal

Based on the dimensions of the wanted targets, two types of object removal are applied: removal of objects with a large horizontal size and removal of objects with a small height.

1) Removal of objects with a large horizontal size

Especially the residuals from the ground reflection are detected as objects with a large horizontal size per depth slice and can be removed from the 3D image volume. In order to avoid the possible removal of wanted target images that are merged with clutter images in one or more depth slices, the limits for the horizontal size of objects are set with a sufficient margin.

2) Removal of objects with a small height

The most striking property of wanted targets is the appearance in several depth slices. The height limit is based on the height of the smallest and weakest wanted target image. The overall result after size-based clutter removal is shown in Fig. 3, where the amount of clutter objects is decreased with 70% to 112 in the surveillance volume.

B. Feature extraction

Feature extraction is a preparatory step for classification. The features are divided into three categories: statistical, structure and shape based features. The statistical and structure based features are computed from intensity images and are therefore computed by using a 3D window around the detected objects [7]. The shape-based features are computed from binary images.

The quality of a feature depends on its discriminating power, reliability and independency with other features. 9 features have been selected:

Statistical based features	Structure based features	Shape based features
F_1. maximum intensity	F_5. similarity with a template	F_8. eccentricity
F_2. ratio of mean over maximum intensity	F_6. similarity between orthogonal horizontal cross lines	F_9. ratio of minor axis over major axis lengths
F_3. ratio of minimum over maximum intensity	F_7. depth similarity.	
F_4. standard deviation.		

C. Classification

For computation reasons the best performing features of the total feature set are selected to be used in the classification process. The classification boundary is calculated from the training set, which is used to decide whether the test object is a wanted target or a clutter object. To minimize the risk of having a missed detection, the boundary is computed with a certain safety margin, which is 5% of the overall maximum value of the specific feature. In Fig. 4 two features (F_2 and F_5) are plotted including the computed boundaries, showing that the boundaries eliminate many clutter objects. The final resulting feature set contains of 5 features F_1, F_2, F_5, F_6 and F_9. After classification, 20 false alarm objects are left in the image volume as can be seen in Fig. 5, which means a clutter reduction of 80%. Because of the down-range resolution close objects are merged into one object image.

V. PERFORMANCE OF THE ALGORITHM

The results of the classification method are shown in a confusion matrix in Table I. It demonstrates that for this 3D image the amount of clutter images classified as wanted targets (false alarms), has been drastically reduced to 18 with a positive detection of 12 wanted targets. The 6 small M14 mines are classified as wanted target. The one missed detection is an 'easy to detect' PMN mine, which is situated too close to the border of the measurement area for appropriate SAR processing.

The above reported results are obtained by using the leave-one-out method to create larger training sets, but a consequence is that the test sets are not completely independent from the training sets. Therefore, the reliability of the established classification boundaries is tested with data from the other transmit/receive antenna combinations. In total, 3 test sets are used: one where the receive antenna is also in mono-static mode as the used data and two with the receive antenna in bi-static mode. The classification results for a bi-static set up are worse than those for mono-static, because bi-static reflections are weaker and distances between transmit and receive antennas are larger. Classification based on the mono-static mode of operation now resulted into one missed detection caused by its weak reflections due to the preprocessing performed on the data. In general, the data measured in mono-static mode gives better results and satisfies the established classification boundaries better.

When overlooking the results, we have to take into account that the data was measured on a fixed type of ground with two types of mines buried using one acquisition scheme. When measuring on a more lossy type of ground than the dry sandy lane, the results may degrade. Besides the circular shape of the buried landmines, other shapes are possible which changes the properties of the landmines. Consequently, the features that are used in the classification scheme probably will then not act properly, causing a reduced performance of the classification procedure. The size of the measured area also influences the outcome of classification. Measuring a larger area results in a larger training set.

VI. CONCLUSIONS AND RECOMMENDATIONS

An algorithm for landmine detection in 3D GPR images is developed, where full use is made of the 3D GPR images. It consists of two procedures: object detection based on a self-developed adaptive thresholding technique and object classification using a simple classification routine to reduce the possibility of missed detections. This algorithm has not only been realized, but also tested and validated.

Landmine detection in 3D GPR images gives promising results. All M14 mines are detected and classified as wanted target and one PMN mine is misclassified due to incorrect SAR processing at the border of the measurement area. Size based clutter removal with the removal of objects with a small height proves to be a good procedure to eliminate clutter from the image volume. However, we have to implement this procedure with care since it may happen that small and deeply buried landmines are removed.

The object detection procedure still needs an expert decision; however this decision could in future be determined by the size and possible depth of the buried landmines. The classifier in the object classification procedure is quite simple, but effective. When paying more attention to the selection of the classification method, it might be better to use a neural network as classifier, which 'learns' to separate landmines from clutter based on their radar images. The performance of a landmine detection system is also improved by combining different sensors; sensor fusion. Merging different sensors like the metal detector, the infrared detector and GPR into one landmine detection system [2] leads to the necessary development of new algorithms.

REFERENCES

[1] Yarovoy, A.G., V. Kovalenko, F. Roth, L.P. Ligthart, R.F. Bloemenkamp (2003), "Multi-Waveform Full-Polarimetric GPR Sensor for Landmine Detection: First Experimental Results," *Int. Conf. Requirements and Technologies for the Detection, Removal and Neutralization of Landmines and UXO, 15-18 September 2003,* Brussels, Belgium, p. 554-560.

[2] Cremer, F., W. de Jong, K. Schutte (2003), "Fusion of Polarimetric Infrared Features and GPR Features for Landmine Detection," *2nd International Workshop on Advanced GPR,* 14-16 May 2003, Delft, The Netherlands, p. 222-227.

[3] Zanzi, L., M. Lualdi, H.M. Braun, W. Borisch, G. Triltzsch (2002), "An Ultra High Frequency Radar Sensor for Humanitarian Demining Tested on Different Scenarios in 3D Imaging Mode," *9th International Conference on Ground Penetrating Radar, Proceedings of SPIE, vol. 4758, 2002, p. 240-245.*

[4] Yarovoy, A.G., V. Kovalenko, F. Roth, J. van Heijenoort, P. Hakkaart, W. de Jong, F. Cremer, J.B. Rhebergen, P.J. Fritz, M.A. Ouwens, R.F. Bloemenkamp (2002), "Multi-Sensor Measurement Campaign at TNO-FEL Test Lanes in July 2002," *Int. Conf. Requirements and Technologies for the Detection, Removal and Neutralization of Landmines and UXO, 15-18 September 2003,* Brussels, Belgium, p. 208-215.

[5] Yarovoy, A.G., L.P. Ligthart, A. Schukin, I. Kaplun (2002), "Polarimetric Video Impulse Radar for Landmine Detection," *Subsurface Sensing Technologies and Applications,* vol. 3, no. 4, October 2002, p. 271-293.

[6] Groenenboom, J., A.G. Yarovoy (2002), "Data Processing and Imaging in GPR System Dedicated for Landmine Detection," *Subsurface Sensing Technologies and Applications*, vol. 3, no. 4, October 2002, p. 387-402.

[7] Ligthart, E.E (2003), *Landmine Detection in High Resolution 3D GPR Images*, MSc. Thesis, Delft University of Technology, Faculty of Electrical Engineering, Mathematics and Computer Science, Delft, The Netherlands.

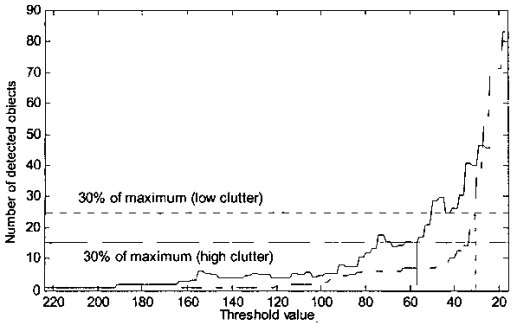

Figure 1. Number of detected object images versus threshold

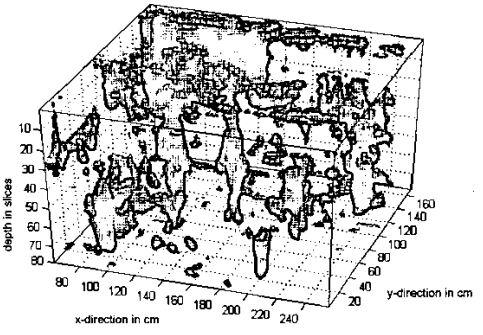

Figure 2. Binary 3D image volume; threshold value 30%

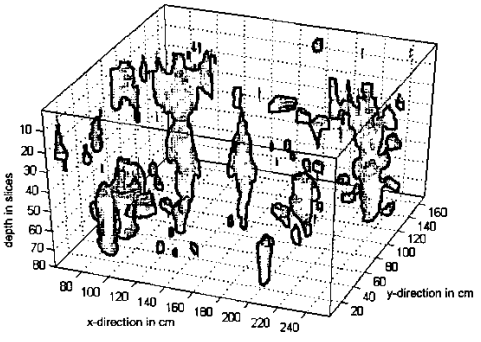

Figure 3. Binary 3D image volume; size-based clutter removal

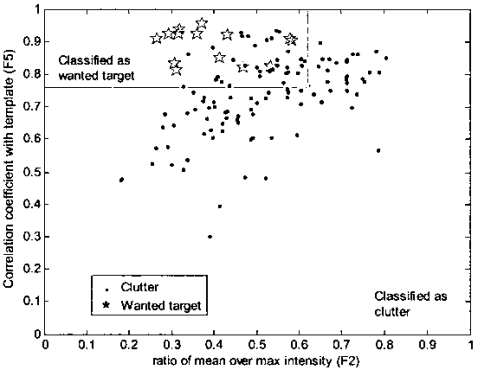

Figure 4. F_2 and F_5 scatter plot and classification boundary

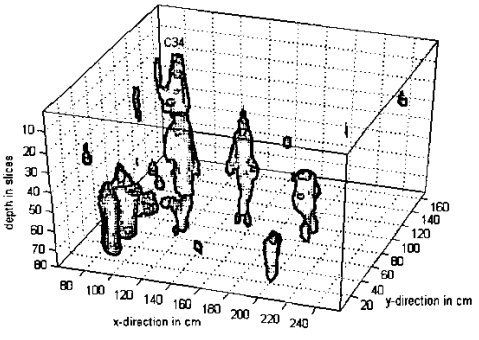

Figure 5. Binary 3D image volume; after classification

	Classified as wanted target	*Classified as clutter*
True wanted target	12	1
True clutter	18	93

Table I. Confusion matrix of the results